Velocity matching and Poiseuille pipe flow of superfluid helium

David C. Samuels
Center for Turbulence Research, Stanford University, Stanford, California 94305
(Received 30 March 1992; revised manuscript received 19 June 1992)

We show that in laminar pipe flow of helium II with the average normal-fluid and superfluid velocities in the same direction, a single superfluid vortex filament can form a series of large vortex rings oriented with the flow. These rings interact to form an array of vortex rings that gives the superfluid a parabolic velocity profile matching the normal-fluid velocity profile. We conclude with some generalizations of this behavior to other flow geometries.

I. INTRODUCTION

Helium below the λ transition (2.17 K at vapor pressure), called helium II, is most successfully described as a superposition of two fluids: a normal fluid with a small but nonzero viscosity η and a superfluid with zero viscosity. Each fluid has its own density (ρ_n and ρ_s) and its own velocity field ($\mathbf{V}_n$ and $\mathbf{V}_s$). At low velocities the two fluids are independent. At high velocities the two fluids appear to be coupled together, with the coupling beginning sharply at some critical values of V_n and V_s.[1] Experiments on flows with $\mathbf{V}_n$ and $\mathbf{V}_s$ parallel have given results that indicate that the coupled state may behave as a single Navier-Stokes fluid with density $\rho=\rho_n+\rho_s$ and the viscosity of the normal fluid.[2,3] One interpretation of these results is that the superfluid velocity field is somehow driven to match the normal-fluid velocity field. The coupling between the two fluids is universally believed to be due to the presence of quantized vortex filaments in the superfluid, which scatter the excitations that make up the normal fluid. The behavior of superfluid vortex filaments in counterflow (where $\mathbf{V}_n$ and $\mathbf{V}_s$ are antiparallel) and in pure superflow ($\mathbf{V}_n=\mathbf{0}$) has been extensively investigated,[4-6] but little is known about the coflowing case ($\mathbf{V}_n$ and $\mathbf{V}_s$ parallel). In recent years there has been renewed interest in employing coflowing superfluid helium to study classical fluid turbulence.[7] In this paper we examine by numerical simulation a simple coflowing case: that of pipe flow with a laminar normal-fluid velocity profile.

II. SIMULATION METHODS

The equation of motion for a superfluid vortex filament[8] is

$$\frac{d\mathbf{S}}{dt}=\mathbf{V}_s+\mathbf{V}_v+\alpha\mathbf{S}'\times(\mathbf{V}_n-\mathbf{V}_s-\mathbf{V}_v)-\alpha'\mathbf{S}'\times[\mathbf{S}'\times(\mathbf{V}_n-\mathbf{V}_s-\mathbf{V}_v)]\ , \tag{1}$$

where $\mathbf{S}$ is the position of a point on the superfluid vortex filament, $\mathbf{V}_s$ is a potential flow imposed from some outside source, $\mathbf{V}_v$ is the velocity field due to all superfluid vortices in the fluid, and $\mathbf{S}'=d\mathbf{S}/d\xi$, where ξ is the arc length. α and α' are temperature-dependent coefficients of the mutual friction. Since α' is significantly smaller than α in the temperature range of interest, we drop the α' term for simplicity. The vortex velocity field $\mathbf{V}_v$ is defined by the Biot-Savart law

$$\mathbf{V}_v(\mathbf{S})=\frac{\kappa}{4\pi}\int\frac{(\xi-\mathbf{S})\times d\xi}{|\xi-\mathbf{S}|^3}\ , \tag{2}$$

where κ is the quantized circulation of the superfluid vortex filament. This integral is taken over all superfluid vortex filaments in the fluid.

We consider only the evolution of the superfluid vortex filaments. The normal-fluid velocity field is treated as an input to the simulations and, in the work reported in this paper, is modeled as an unchanging velocity field. The response of the normal fluid to the superfluid vortex filaments is an interesting subject that should be pursued in future studies.

In our simulations each superfluid vortex filament is represented numerically by a series of nodes connecting straight vortex segments. The singularity in the Biot-Savart law is handled by a method due to Schwarz.[8] The equation of motion [Eq. (1)] is solved by the Runge-Kutta-Fehlberg method. In order to allow for growth and shrinkage of the vortex filament during the simulation, mesh nodes are added or removed at each time step so that the ratio of the local mesh size to the local radius of curvature of the filament is kept approximately constant. A typical value of this ratio is $2\pi/64$ over a range of radius of curvature from R to $0.01R$, where R is the length scale of the computational volume.

When two vortex filaments cross, we assume that a reconnection occurs, changing the topology of the filaments. In this simulation a reconnection is made whenever the distance between a node n_i and a nonadjacent node n_k is less than the distance between the node n_i and its neighbor n_{i+1} along the filament in the direction of the filament vorticity. The physical process behind the reconnection of superfluid vortex filaments is unknown, and this reconnection assumption is a possible difficulty with all superfluid-vortex-filament simulations. It is a surprising conclusion of this simulation that, in striking contrast to the counterflow simulations[4] where vortex reconnection is necessary for stability of the vortex tangle, reconnection plays a minor role, if any, in this lami-

nar coflow. We allow reconnections to occur, but they rarely happen, and the overall behavior of the system is unaffected by their presence or absence.

We initiate each simulation with a small length of vortex filament present in the superfluid. Typically, this initial vorticity takes the form of a small vortex loop attached to a boundary. We are not dealing with the problem of the *intrinsic* nucleation of vorticity (i.e., the spontaneous generation of vortex filaments in a vortex-free flow).[9] We are instead dealing with the much simpler problem of *extrinsic* nucleation, which is defined as the growth of a large length of vortex filament from an existing small amount of vortex filament. This initial vorticity has been detected experimentally[10] and is most likely to be present as vortex filaments pinned to roughness on the boundaries. This pinning is not modeled in our simulation since the flow velocities used are greater than the small velocity needed for depinning.[8]

III. VELOCITY MATCHING

A normal-fluid velocity field with a nonzero gradient allows a more interesting behavior of individual superfluid vortex filaments than does a uniform velocity field. Specifically, if there is a region of the fluid flow where $\mathbf{V}_n=\mathbf{V}_s$ initially and there are also regions of the flow where $\mathbf{V}_n\neq\mathbf{V}_s$, then superfluid vortex growth by mutual friction may occur in the latter region and filaments with circulation parallel to the normal-fluid circulation of the region of equal velocity will be transported toward that region by the mutual friction force. In response to the mutual friction force, these vortex filaments will accumulate near the surface of the equal-velocity region with such a density as to match the local $\mathbf{V}_n$ field with the combined superfluid velocity fields of the quantized vortex filaments, thus increasing the size of the region where the velocities are matched. This behavior is not dependent on the exact form of the mutual friction force. It requires only that the mutual friction force be a function of the local relative velocity $\mathbf{V}_n-\mathbf{V}_s$ with a positive component in the $\mathbf{V}_n-\mathbf{V}_s$ direction.

A familiar example of this velocity matching is the classic rotating-bucket experiment.[11] In this situation the centerline of the bucket acts as the accumulation point where $\mathbf{V}_n=\mathbf{V}_s$. Superfluid vortices are presumably formed at the outer boundary of the bucket and move in toward the centerline.[12] As the superfluid vortex filaments accumulate with the appropriate density, the superfluid and normal-field velocity fields become matched and the final flow throughout the bucket is that of a classical fluid over distances greater than the average vortex filament spacing.

Another example of this behavior is laminar pipe flow. At sufficiently low Reynolds numbers and in the absence of quantized vortices, the flow of helium II through a pipe should be described by a superfluid flow with a flat velocity profile V_{s0} that slips at the walls and by a normal-fluid flow with a parabolic velocity profile (Poiseuille flow)

$$V_n(r)=2V_{n0}[1-(r/R)^2]\ , \tag{3}$$

where V_{n0} is the average normal-fluid flow and R is the pipe radius (Fig. 1). The relative velocity of the two fluids is zero at a radius r_0 given by

$$r_0=R\left[1-\frac{V_{s0}}{2V_{n0}}\right]^{1/2}\ . \tag{4}$$

For the simple case of $V_{s0}=V_{n0}$, this radius is $r_0=R/\sqrt{2}$. We will refer to the cylindrical surface described by r_0 as the "nodal" surface.

IV. REPEATED VORTEX GENERATION

Because of the no-slip boundary condition on the normal fluid, the normal-fluid velocity near the wall is much smaller than the superfluid velocity. Thus the relative velocity $\mathbf{V}_{ns}=\mathbf{V}_n-\mathbf{V}_s$ near the wall points in the direction opposite to the average flow. A small vortex half ring connected to the pipe wall and oriented against the average flow direction (with the local $\mathbf{V}_{ns}$) will grow in response to the mutual friction force. Rings with self-induced velocity larger than $\mathbf{V}_{ns}$ will not grow, but these rings are very small [$r\leq O(0.01R)$] for the range of flow velocities considered in this paper. Typically, we begin our simulations with a vortex half ring of radius $r=0.1R$. This choice is made for clarity of the evolution of the vortex filament. The process that we describe below will also occur for a large initial vortex loop, but it will then have a more complicated initial transient behavior.

Since the relative vorticity V_{ns} changes sign at r_0, the half ring will not grow through the nodal surface into the center region of the pipe, but will continue to grow in the outer region until the two ends of the vortex meet on the opposite side of the pipe (Fig. 2). The relative axial velocity inside the nodal surface acts as a barrier through the mutual friction term $\alpha\mathbf{S}'\times(\mathbf{V}_n-\mathbf{V}_s)$ in the equation of motion [Eq. (1)]. Unless the initial half ring is exactly in the plane perpendicular to the flow, the ends of the vortex at the pipe boundary will pass each other before the vortex cores touch. By the reconnection assumption, the vortex filament will then reconnect, forming a large vortex ring oriented with the flow and leaving another small half ring connected to the pipe wall to continue the pro-

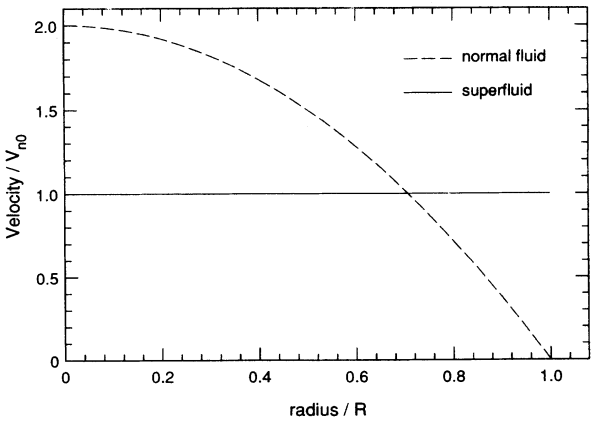

FIG. 1. Superfluid and normal-fluid velocity profiles in laminar pipe flow with no superfluid vortex filaments.

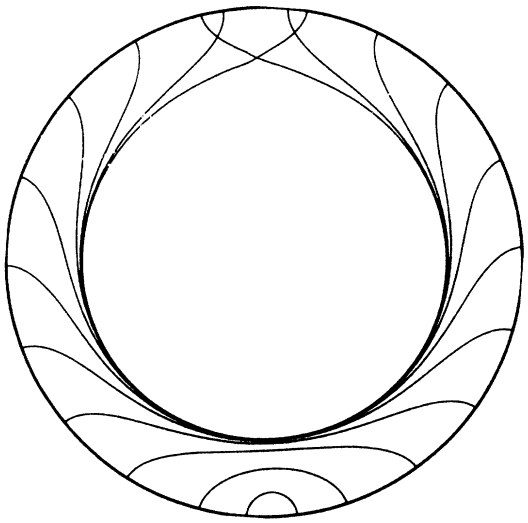

FIG. 2. Time lapse growth of a superfluid vortex filament in the spanwise plane of the pipe. The initial state is the half ring at the bottom of the figure. The filament does not grow through the nodel surface into the center of the pipe.

cess repeatedly. Thus the parabolic profile of the normal-fluid velocity allows a vortex generator to operate in pipe flow. The results of this process are shown in Fig. 3. Here the vortex generator has produced three rings and is beginning to generate a fourth as it moves upstream. The flow is in the negative-Y direction, and all coordinates are in the rest frame of the superfluid average velocity. The simulation was initiated with a small half ring attached to the pipe boundary at $Y=0$, $X=0$, and $Z=-R$ and oriented against the average flow. The rings generated lie nearly on the nodal surface, are oriented with the average flow, and are tilted in the streamwise direction by the movement of the generator during their formation.

It is important to note that this vortex generator does not involve any pinning of the vortex to the boundary and does continue to operate at high flow velocities where pinning is negligible.[8,13] Other proposed vortex generations depend on pinning in some way for their operation.[14,15]

In this description of the action of the vortex generator, we have employed the reconnection assumption. While this simplifies the numerical simulation by limiting the amount of filament in close proximity, it is not a necessary part of the physical behavior in this case. In a vortex tangle[4,8] produced by a counterflow, reconnections mainly occur between filaments at random orientations and with noncorrelated velocities. These reconnections lead to large changes in the vortex topology and create regions of locally high curvature, which greatly affect the motion of the vortex filament. Reconnections are a critical limitation on the line density in vortex tangles.[4] The reconnections for the vortex generator described above are of a much less dynamic nature in comparison to the tangle reconnections. Primarily, the reconnections are always occurring between nearly parallel filaments (Fig. 4) and thus make little change in the filament's curvature or motion. Second, the filaments that reconnect are approaching each other slowly, since their velocities are very similar, and the time of reconnection is not expected to be simulated accurately by the model employed here. Because these reconnections make little change in the filament's motion, we do not expect this inaccuracy in the timing to have any effect on the overall behavior of the filaments. If reconnections were to be ignored, or greatly delayed, the two legs of the vortex generator would independently produce a pair of helical vortex filaments near the cylindrical nodal surface. The average superfluid velocity field of a large number of these helical filaments would be the same as the average velocity field of a large number of vortex rings.

Since the reconnections are unimportant to the vortex

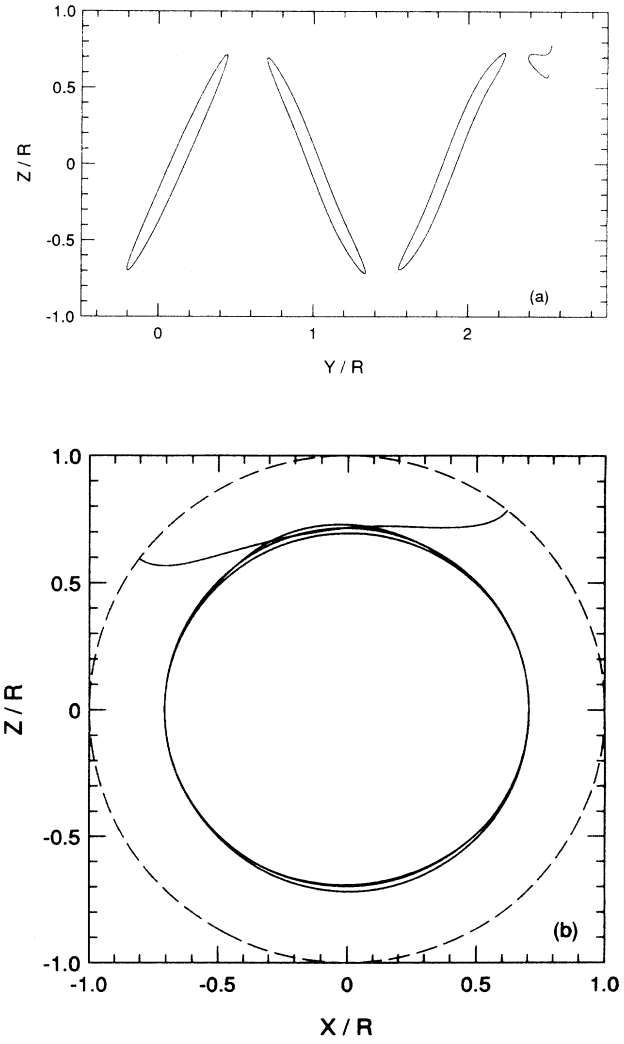

FIG. 3. (a) Streamwise view of three vortex rings produced by the generator. Simulation variables are $\alpha=0.2$ and $\tilde{V}_n=-160$ along the Y axis. The initial angle of the generator was $0.1\pi/2$ from the spanwise plane. The dotted lines denote the nodal surface. This vortex generator is in the upper right corner. All disconnected filament ends are attached to the pipe wall. (b) Spanwise view of the vortex rings. The dashed line denotes the pipe boundary. The vortex generator is at the top of the figure, attached to the pipe wall.

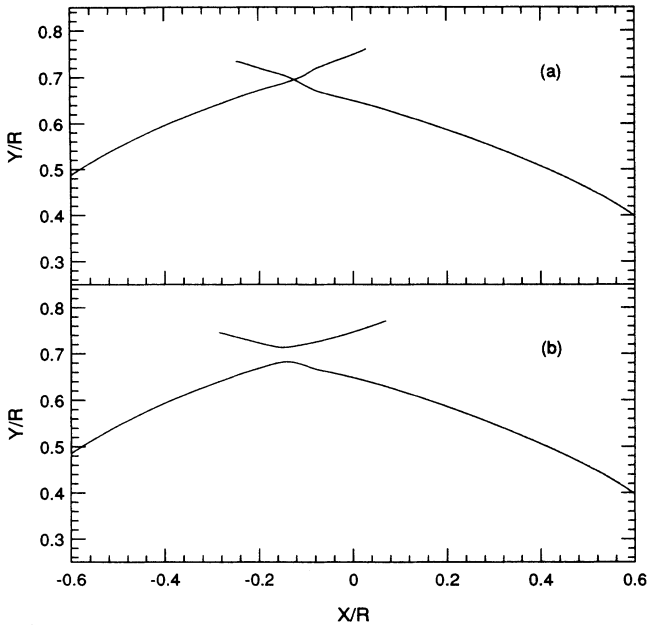

FIG. 4. Sample reconnection of the generator legs: (a) before reconnection and (b) five time steps after reconnection.

motion, the vortex generator is very robust. Each leg of the generator moves independently, and any change in the motion of one leg, caused by some surface irregularity, for example, will only shift the time of reconnection to form the ring. Similarly, the independence of the legs allows many generators to operate simultaneously in very close proximity. The legs of separate generators interact in the same manner as the two legs of a single generator, producing a more distorted ring. This is demonstrated in Fig. 5, which shows the results of a simulation initiated with three coplanar vortex generators. Each of the three initial vortex half rings was identical to the initial half ring in the simulation of Fig. 3, but separated in the spanwise plane by an angle of 120°. The flow conditions were identical to the simulation of Fig. 3. Figure 5 shows the vortex filaments after two complete rings have been generated. Each of the rings was made partially by each of the three generators. The resulting vortex rings are more closely spaced and lie more in the spanwise plane than the rings produced by single generators. In general, we expect the interactions of a larger number of vortex generators to produce closely spaced rings which are reasonably flat in the spanwise plane.

In Fig. 6 we give the frequency of ring production from the single vortex generator for a few values of α and with a constant ratio $V_{s0}/V_{n0}=1$. Of course, for rings produced by multiple vortex generators, the frequency is multiplied by the number of generators involved. These frequencies were taken from the simulations by measuring the angular velocity of one leg of the vortex generator along the pipe wall. For low-frequency generators, this angular velocity was not constant over distances on the order of πR and so these values were not measured. Despite this, it is clear from Fig. 6 that there is an α-dependent minimum velocity for the operation of the vortex generator. Below this minimum velocity, the initial vortex half ring grows to a stable configuration. This stable configuration will be considered in the future.

The velocities and frequencies in Fig. 6 are given in dimensionless form. For the velocity scale, we have chosen the value

$$V_{\text{scale}}=\frac{\kappa}{4\pi R}\ln\left[\frac{8R}{a_0}\right], \tag{5}$$

where a_0 is the superfluid-vortex-filament core parameter ($a_0\simeq 1$ Å). For the frequency scale, we have

$$f_{\text{scale}}=V_{\text{scale}}/R\ . \tag{6}$$

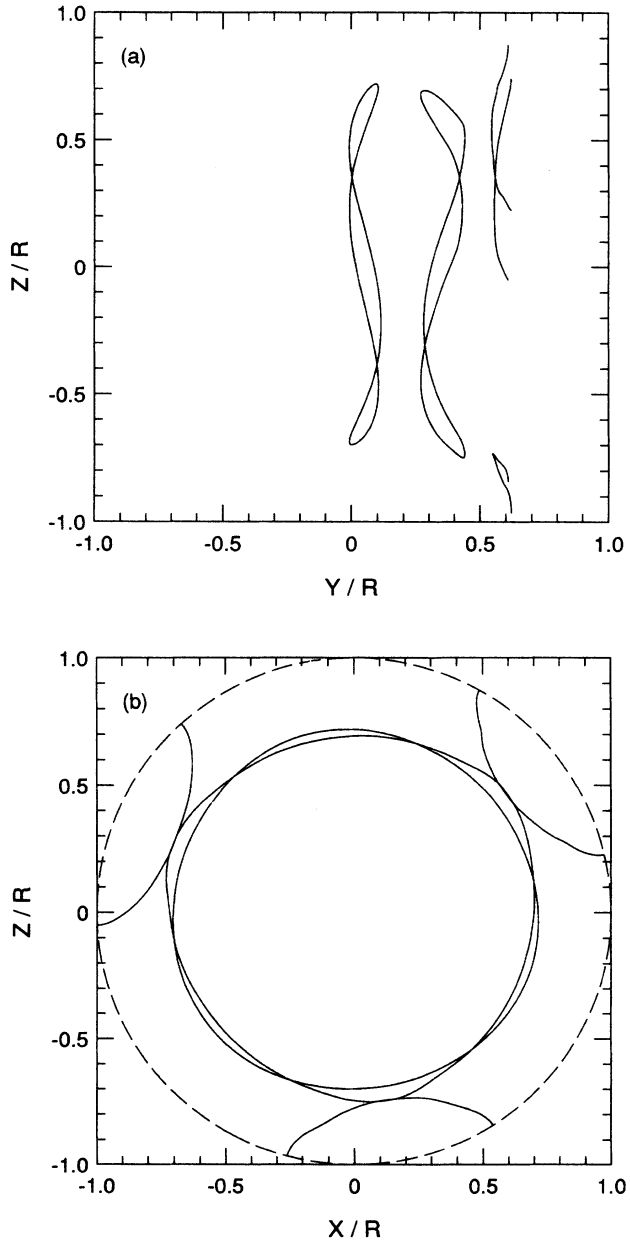

FIG. 5. (a) Streamwise view of two vortex rings produced by three interacting generators. Simulation variables are the same as in Fig. 3. (b) Spanwise view of the vortex rings and generators. The dashed line denotes the pipe boundary.

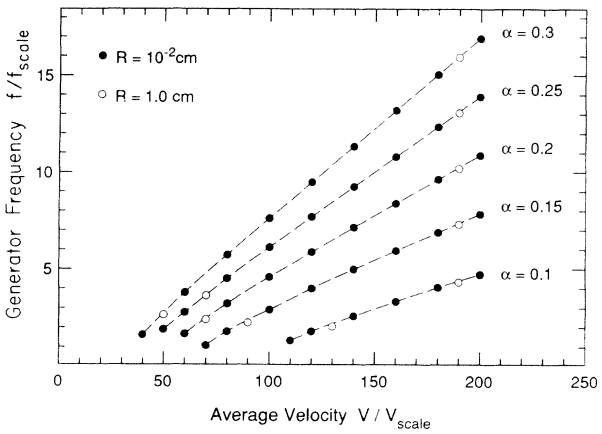

FIG. 6. Frequency of ring generation by a single vortex generator over a range of α. See text for the velocity and frequency scales. Lines are drawn to guide the eye.

We will denote nondimensionalized variables with a tilde. Simulations conducted with different values of R confirm the validity of this choice of scales. The Reynolds number, written in terms of the nondimensionalized velocity, is

$$\mathrm{Re}=\frac{\rho R V}{\eta}=\frac{\rho \tilde{V}\kappa}{\eta 4\pi}\ln\left[\frac{8R}{a_0}\right]\approx 10\tilde{V}\ . \tag{7}$$

To remain in the laminar flow regime, we limit $\tilde{V}_{n0}$ to 200 and less. For wide pipes this maximum velocity is very small (0.3 cm/sec for $R=1$ cm), but for the small capillaries commonly used in experiment[1,13] the maximum velocity is reasonably high (25 cm/sec for $R=0.01$ cm). Since we will show that a parabolic velocity profile forms for the superfluid as well as the normal fluid, we define the Reynolds number with the total density ρ.

The presence of a surface with $\mathbf{V}_n=\mathbf{V}_s$ in the fluid allows the generator to operate, and so this vortex generation occurs only in the range $0<V_{s0}/V_{n0}<2$ (see Fig. 1). These limits are only outer limits since, for V_{s0}/V_{n0} near 2, the local velocity difference $\mathbf{V}_n-\mathbf{V}_s$ in the inner section of the pipe may be too small to prevent the vortex filament from crossing the pipe axis by its own self-induced velocity and for V_{s0}/V_{n0} near 0 the velocity difference at the pipe boundary may be too small to cause the generator to grow. For this paper we will mainly consider the case $V_{s0}=V_{n0}$.

V. VORTEX-RING INTERACTIONS

When initially created by the vortex generator, the rings lie on or near the nodal surface and are elongated in the direction of the flow (Fig. 3). This elongation is lower at high flow velocities, as the vortex generator forms rings more rapidly, and is also reduced if the ring is produced by multiple generators. Through mutual friction these elliptical rings eventually relax to circular rings in the plane perpendicular to the flow. Since the vortex generators produce a large number of rings with the same orientation, the interactions between the rings will be non-negligible. With the large number of rings and the necessity of including the full nonlocal interactions, a simulation of the detailed vortex core motion is not practical at this time. Instead, we use a simple concentric-ring model, where each ring produced by the vortex generator is modeled as a flat circular ring in the spanwise plane, concentric about the pipe axis. The circular rings interact through the Biot-Savart law, and the superfluid boundary conditions (impenetrable walls with slip) are satisfied approximately by image vortex rings with radius and circulation

$$r_{\mathrm{image}}=R^2/r_{\mathrm{ring}}\ , \tag{8a}$$

$$\kappa_{\mathrm{image}}=-\frac{R}{r_{\mathrm{ring}}}\kappa\ . \tag{8b}$$

This choice for the form of the image vortex rings was made in order to satisfy most closely the boundary conditions near the streamwise position of the vortex ring. The presence of a number of randomly spaced vortex generators is simulated by adding rings periodically at random streamwise positions along the pipe, with a ring radius equal to the radius where $\mathbf{V}_n=\mathbf{V}_s$ locally. Periodic boundary conditions are used in the direction of the flow to simulate an infinite pipe. The velocity fields of the superfluid vortex rings were precalculated and used in the simulation as a set of lookup tables. The axial (or streamwise) position (y) and radius (r) of each ring were calculated by the Runge-Kutta-Fehlberg method with the equations of motion,

$$\frac{dy}{dt}=V_{\mathrm{ring}}+V_{s,\mathrm{app}}+V_{Vy}+V_{Iy}+\alpha(V_{Vr}+V_{Ir}) \tag{9a}$$

and

$$\frac{dr}{dt}=V_{Vr}+V_{Ir}+\alpha(V_n-V_{\mathrm{ring}}-V_{s,\mathrm{app}}-V_{Vy}-V_{Iy})\ , \tag{9b}$$

where V_{ring} is the velocity of a superfluid vortex ring of radius r in an unbounded fluid, $V_{s,\mathrm{app}}$ is an applied superfluid velocity field which is constant across the diameter of the pipe, V_{Vy} and V_{Vr} are the components of the superfluid velocity field summed over all other vortex rings in the fluid, and V_{Iy} and V_{Ir} are the components of the superfluid velocity field summed over all image vortex rings. For this example, α was chosen to be 0.15, corresponding to a temperature of approximately 1.8 K.

The applied superfluid velocity field $V_{s,\mathrm{app}}$ is an important boundary condition of this simulation. It must be stressed that $V_{s,\mathrm{app}}$ is not the average superfluid flow through the pipe. The combined velocity fields of the image vortex rings produce a net flow against the applied flow $V_{s,\mathrm{app}}$. This backflow is analogous to the uniform magnetic field inside a selonoid, with the image vortex rings representing the current loops. In order to keep a constant average superfluid flow (which is our chosen boundary condition for this simulation), the average velocity field of the vortex rings and their images must be calculated and $V_{s,\mathrm{app}}$ increased to compensate. To calculate the required change in $V_{s,\mathrm{app}}$, a simple model for the total superfluid velocity profile $V_s(r)$ was used. We ob-

served from simulations with constant $V_{s,\mathrm{app}}$ that $V_s(r)$ always had a simple form, which is illustrated schematically in Fig. 7. Qualitatively, $V_s(r)$ could be described by a continuous function across three sections of the pipe radius. For small radii, where no vortex rings existed, $V_s(r)$ is constant. For a range of median radii, where a vortex-ring array existed (see discussion below), $V_s(r)$ approximately matched the normal-fluid velocity profile. And for large radii, where again no vortex rings existed, $V_s(r)$ was also constant. With this simple model, the average superfluid velocity $V_{s,\mathrm{av}}$ can be calculated from measurements of the average superfluid velocity along the pipe axis, $V_{r=0}$, and along the pipe wall, $V_{r=R}$, by

$$V_{s,\mathrm{av}}=\frac{1}{\pi R^2}\int_0^{2\pi}\int_0^R rV_s\,dr\,d\theta$$
$$=V_{r=0}-\frac{1}{4V_{n0}}(V_{r=0}^2-V_{r=R}^2)\ . \tag{10}$$

The velocities $V_{r=0}$ and $V_{r=R}$ were calculated from the average of ten equally spaced positions along the pipe. These average velocities were used in Eq. (10) to update the applied superfluid velocity at every time step by the formula

$$V_{s,\mathrm{app}}(t+\Delta t)=V_0+[V_{s,\mathrm{app}}(t)-V_{s,\mathrm{av}}(t)]\ , \tag{11}$$

where V_0 is the desired constant average superfluid flow rate.

When the vortex density is small, the vortex rings actually repel each other through the mutual friction force. Consider a pair of vortex rings with equal radius r_0 (where $\mathbf{V}_n=\mathbf{V}_s$) and oriented along the pipe axis in the direction of the flow. Initially, the lead ring will grow in radius and the lagging ring will shrink, as is expected for a pair of vortex rings with a common axis of symmetry.[14] If the rings are far enough apart, this process will be halted by the increasing mutual friction force due to the increasing relative axial velocity $(\mathbf{V}_n-\mathbf{V}_s)$ as the rings move away from r_0. In addition, the mutual friction force on each ring due to the radial superfluid velocity field of the other ring (αV_{Vr}) will cause a repulsive velocity between the rings. Thus, in this case, the "leapfrog"

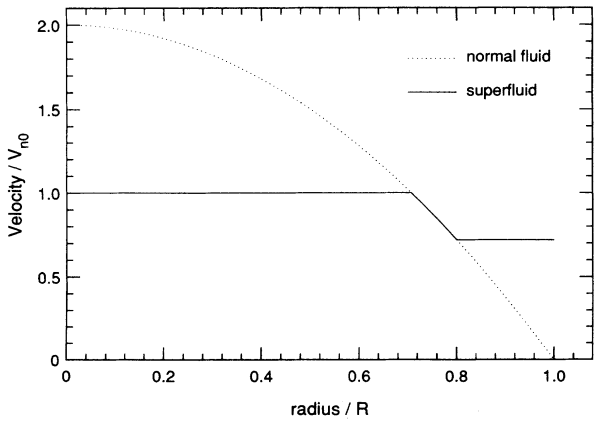

FIG. 7. Model of $V_s(r)$ used to calculate the average superfluid flow rate.

behavior[16] expected of the vortex rings does not always occur. This repulsive motion becomes attractive within some distance (where the repulsive motion due to mutual friction is overcome by the attractive motion due to the ring's change of radius), and the vortex rings stabilize at a separation

$$\frac{\delta}{R}\approx\frac{1}{R}\left[\frac{\kappa}{\omega_n(r)}\right]^{1/2}=\left[\frac{\kappa}{4V_{n0}r}\right]^{1/2}, \tag{12}$$

where $\omega_n(r)$ is the normal-fluid vorticity at the radius r. At this separation the local $\mathbf{V}_{ns}$ at each ring is approximately zero, the mutual friction force is negligible, and the two rings leapfrog each other. Therefore, if the vortex-generator frequency is low enough to form widely spaced rings, these rings will separate [Fig. 8(a)] until a generator produces a ring within the attractive distance of a ring produced by another generator. Because of the combined velocity fields of the two image rings, this pair of rings will move along the pipe axis with a different velocity than any single ring and will thus gather more rings, forming a toroidal vortex array [Fig. 8(b)]. Alternatively, if the vortex-generator frequency is high enough to produce the rings initially within the attractive distance, a single generator will form a vortex array. The relative velocity $\mathbf{V}_{ns}$ (averaged over length scales greater than δ) is zero within the vortex-ring array.

The toroidal vortex array which results from this process grows in size until it approaches the pipe wall [Fig. 8(c)]. The influence of the image vortices flattens the vortex array, and the array subsequently grows mainly in length with slow change in radial size [Fig. 8(d)]. Eventually, these arrays merge and grow to extend completely across the periodic computational domain in the direction of the flow [Fig. 8(e)]. Though we use the term "array" to describe the grouping of superfluid vortex filaments, we do not mean to imply that the filaments form a stationary lattice, as they do in a rotating bucket.[17] After the vortex array grows large enough to approach the pipe wall and flatten, we detect no indication of any regular lattice formation.

As this array grows radially, the relative velocity $\mathbf{V}_{ns}$ at the boundary will eventually decrease below a minimum value for the operation of the vortex generator. Associated with this minimum relative velocity is a distance r_c, defined as the distance from the pipe wall to the outer edge of the matched velocity region $(V_{ns}=0)$ formed by the vortex-ring array. The relative velocity at the wall is

$$|V_{ns}(R)|=|0-V_s(R)|\approx 2V_{n0}\left[1-\frac{(R-r_c)^2}{R^2}\right], \tag{13}$$

since the superfluid velocity profile is approximately constant from the outer edge of the matched velocity region to the wall. The self-induced axial velocity of the generator leg may be approximated by the velocity of a vortex ring with radius r_c. When the relative velocity at the boundary is less than this self-induced velocity, the vortex generator will not grow. Therefore this distance r_c is approximately determined by equating the velocity of a

ring of size r_c with the relative velocity at the boundary and solving for r_c:

$$\frac{\kappa}{4\pi r_c}\ln\left[\frac{8r_c}{a_0}\right]=2V_{n0}\left[1-\frac{(R-r_c)^2}{R^2}\right]. \tag{14}$$

Assuming $r_c \ll R$, we have

$$\frac{r_c}{R}=\frac{1}{2}\left[\frac{\kappa}{4\pi R V_{n0}}\ln\left[\frac{8r_c}{a_0}\right]\right]^{1/2}\approx\frac{1}{2}\left[\frac{1}{\tilde{V}_{n0}}\right]^{1/2}. \tag{15}$$

The width r_c is calculated from the flow properties near the wall and is the same for any value of V_{s0}/V_{n0}. Over the velocity range $50<\tilde{V}_{n0}<200$, the ratio r_c/R varies from 7%to 4%. It is instructive to compare this distance with the average spacing δ_R of the vortex array at the pipe wall. From Eq. (12) this spacing is

$$\frac{\delta_R}{R}=\frac{1}{2}\left[\frac{\kappa}{RV_{n0}}\right]^{1/2}, \tag{16}$$

and so

$$\frac{r_c}{\delta_R}=\left[\frac{\ln(8r_c/a_0)}{4\pi}\right]^{1/2}. \tag{17}$$

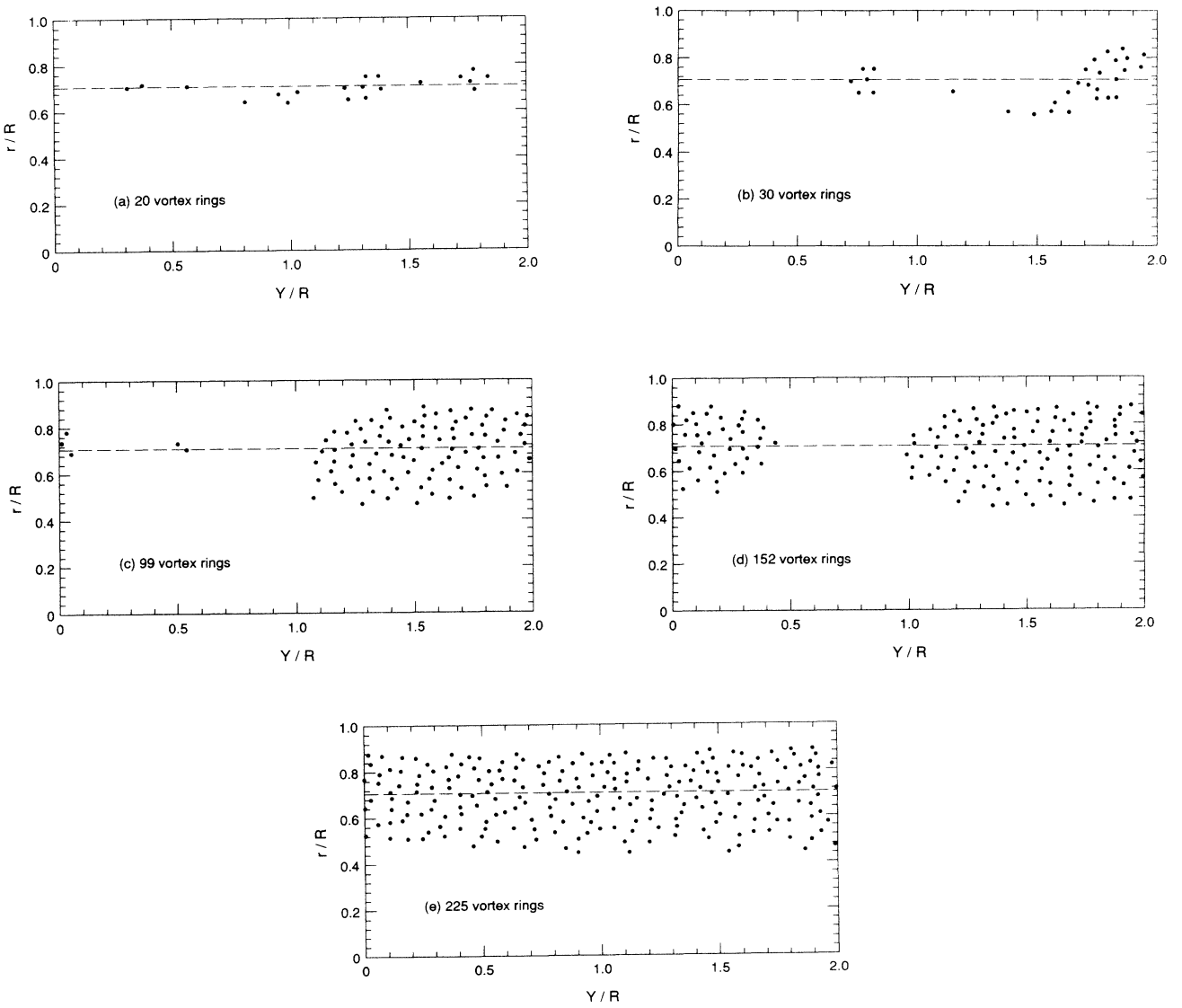

FIG. 8. Radius vs streamwise position of concentric rings in the pipe. Rings are added periodically at random streamwise positions to simulate the vortex generators. The dashed line denotes the nodal surface. The pipe is periodic in the streamwise direction with a length $2R$. The flow velocity is $\tilde{V}=80$ in the positive-Y direction with equal average V_n and V_s. All positions are shown in the rest frame of the average superfluid velocity. (a) At low ring densities, the rings are separated with a small amount of clustering. (b) One cluster of vortex rings begins to dominate. As the clusters become large they come almost to rest in the superfluid rest frame. (c) The vortex cluster grows predominately in the streamwise direction and slowly in the radial direction. (d) The cluster continues to grow, with the fastest growth in the downstream direction (in the average superfluid rest frame). (e) Eventually, the cluster fills the length of the periodic pipe and continues to grow in the radial direction.

Since the logarithmic term in Eq. (17) is on the order of 10 for a wide range of practical r_c, the distance r_c is very nearly equal to one array spacing. The effect of this coincidence is that the final vortex array will appear to have one layer of vortices missing near the boundary. The array of vortices in a rotating bucket also has a vortex-free strip at the boundary. In this case the size of the vortex-free strip is[18]

$$\frac{r_c}{b}=\left[\frac{\ln(b/a_0)}{2\pi}\right]^{1/2}, \tag{18}$$

where b is the mean vortex spacing. The minor differences between Eqs. (17) and (18) are easily understood to be due to the different geometries.

The velocity profiles (Fig. 9) of the normal fluid and superfluid show that by the end of the simulation the velocities in the outer part of the pipe are matched fairly well, though there will always be some slip of the superfluid at the wall due to the cutoff condition for the vortex generator. One should keep in mind that a relatively low flow rate ($\tilde{V}_0=80$) was chosen for this simulation example in order to minimize the number of necessary vortex rings. Also, this simulation was not run far enough for the superfluid vortex array to extend to r_c because of time constraints on the computation. From Eqs. (13) and (15), the completely developed vortex array for this flow rate would extend to a distance of $0.06R$ from the pipe wall and would have a relative velocity at the wall of $0.22\tilde{V}_0$. For higher flow rates, the vortex array spacing will be smaller, giving a smoother match of the two velocity fields and a smaller velocity difference at the boundary.

As a consequence of the slip velocity at the boundary, the vortex array does not extend completely to the center of the pipe. There is a clearly defined "vortex front" bounding the inner surface of the array [Fig. 8(e)]. The position r_i of this stationary vortex front may be calculated by applying the simple three-segment model for $V_s(r)$, with the outer radius of the vortex array defined by $R-r_c$, and solving for the inner radius of the array. This radius is

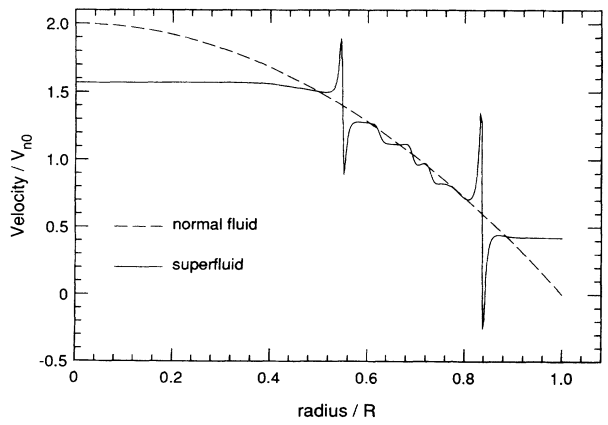

FIG. 9. Normal-fluid and superfluid velocity profiles in the pipe with 225 superfluid vortex rings present. The profiles are taken at $Y=1R$ in Fig. 8(e).

$$\frac{r_i}{R}=\left[1-\frac{V_{s0}}{V_{n0}}+4\left[\frac{r_c}{R}\right]^2-4\left[\frac{r_c}{R}\right]^3+\left[\frac{r_c}{R}\right]^4\right]^{1/4}, \tag{19}$$

where V_{s0} is the average superfluid flow rate. In this formula we have allowed $V_{s0}\neq V_{n0}$. The width of this inner vortex-free region is comparatively large for $V_{s0}<V_{n0}$. Using Eq. (15) in Eq. (19), the ratio r_i/R varies from 36% to 26% over the velocity range $50<\tilde{V}_n<200$ and with $V_{s0}=V_{n0}$. Since the ratio r_c/R is small, the inner vortex-free region disappears quickly for V_{s0} only slightly greater than V_{n0}. This may restrict any practical observation of this region to flows with $V_{s0}<V_{n0}$. The lack of the inner vortex-free region will allow the vortex rings to shrink to zero radius and disappear. This destruction of vortex rings should prevent the vortex array from growing to a radius large enough to suppress the vortex-generator operation, and so we expect flows with $V_{s0}>V_{n0}$ to have continuously operating vortex generators.

VI. COMPARISON TO SOLUTIONS OF THE HALL-VINEN-BEKAREVICH-KHALTNIKOV EQUATIONS

In the Hall-Vinen-Bekarevich-Khalatnikov (HVBK) equations, vorticity is allowed in the superfluid. This vorticity is interpreted as an average over the coarse structure of superfluid vortex filaments. Geurst[19] has shown that solutions of the HVBK equations yield nonuniform superfluid velocity profiles in pipe flow with a parabolic normal-fluid velocity profile. Geurst interprets this V_s profile as the result of the continuous creation of superfluid vortex rings at the outer wall of the pipe and their continuous destruction at the pipe axis, with a constant mutual friction dissipation driving the motion of the rings. Though his paper concentrates on the solutions for nonzero mutual friction dissipation, it is clear that for the special case of zero mutual friction, which is the case for the rings produced by this vortex generator, the resulting superfluid velocity profile consists of continuous segments of uniform velocity and segments of parabolic velocity matching the normal-fluid velocity profile, just as we observe (Fig. 9). Especially interesting in the context of the present work is the range of V_{s0}/V_{n0} for which his theory allows a zero value for the chemical potential gradient μ', which is due to mutual friction. This range is $0<V_{s0}/V_{n0}<2$, in complete agreement with the maximum range of operation of the vortex generator. Remember that the vortex rings produced by the generator are at rest with respect to the local normal-fluid velocity and therefore do not themselves contribute to dissipation by mutual friction, while the operation of the generator does cause dissipation during the formation of each ring. Geurst also gives an analysis of some experimental results by de Haas and van Beelen,[20] which shows the measured μ' is zero in the range $0<V_{s0}/V_{n0}<1.2$ with μ' comparatively small in the range $1.2<V_{s0}/V_{n0}<2$. These results are consistent with the formation of stable vortex-ring arrays (with zero dissipation) for $0<V_{s0}<V_{n0}$ and the continuous operation of

vortex generators (with some dissipation) caused by the lack of an inner vortex front for $V_{s0} > V_{n0}$.

VII. FINITE-LENGTH EFFECTS

We have only considered the idealized case of infinite-length pipes. However, it is well known that the finite length of real pipes has a strong effect on the flow of classical fluids, both from the entry length at the pipe inflow and the flushing of flow disturbances through the pipe outflow. The same is true for helium II. Schwarz[15] has pointed out that since vortex filaments will be convected downstream at approximately the superfluid flow rate, these filaments will be continuously flushed out of a real pipe of finite length. Thus a continuous injection of vortex filaments, presumably at or near the pipe entrance, is necessary to sustain the filament population in any finite pipe. In simulations of a streamwise vortex filament (Fig. 10) in pure superflow ($V_n = 0$) with the pipe inflow simulated by pinning the upstream end of the filament to a fixed position on the cross section of the channel, Schwarz[15] has shown that the streamwise filament is unstable to the growth of a helical wave. The repeated collisions of the growing helical wave with the pipe wall result in the injection into the flow of a succession of vortex loops attached to the pipe wall. We distinguish this type of vortex generator from our unpinned vortex generator described in Sec. IV by calling the former an inflow vortex generator. Though the details of this behavior may be different for pipe flows with nonzero V_n, a similar process occurs in these flows. The vortex loops injected into the pipe by the inflow vortex generators are similar to the vortex loops used to initiate our simulations, and these loops do also evolve in unpinned vortex generators, forming vortex rings, until they are flushed through the pipe outflow.

The presence of a nodal surface does alter the behavior of the Schwarz inflow vortex generators in one obvious way. The upstream end of the vortex filament extends through the pipe inflow at some arbitrary position on the pipe cross section. If this position lies between the nodal surface and the pipe wall [Fig. 11(a)], then the streamwise vortex filament behaves as described by Schwarz. The growing helical wave intersects the pipe wall, injecting a series of unpinned vortex generators into the flow. If, however, this position lies within the nodal surface [Fig. 11(b)], then the growth of the helical wave will stop at the nodal surface (since the instability is driven by the local relative velocity) and will never reach the pipe wall. In this case the downstream end of the filament, which is attached to the pipe wall, acts as a single independent leg of an unpinned vortex generator.

In laminar flow through any finite-length pipe, it is important to consider the entry-length problem. For a classical fluid, an often non-negligible downstream distance Y is necessary for the establishment of the Poiseuille veloci-

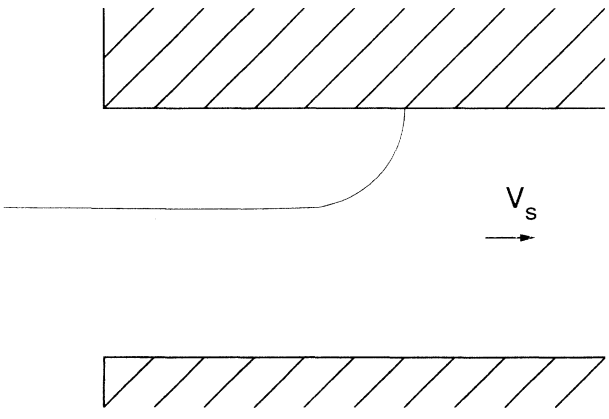

FIG. 10. Geometry of a superfluid vortex filament pulled into a pipe intake by the superfluid flow.

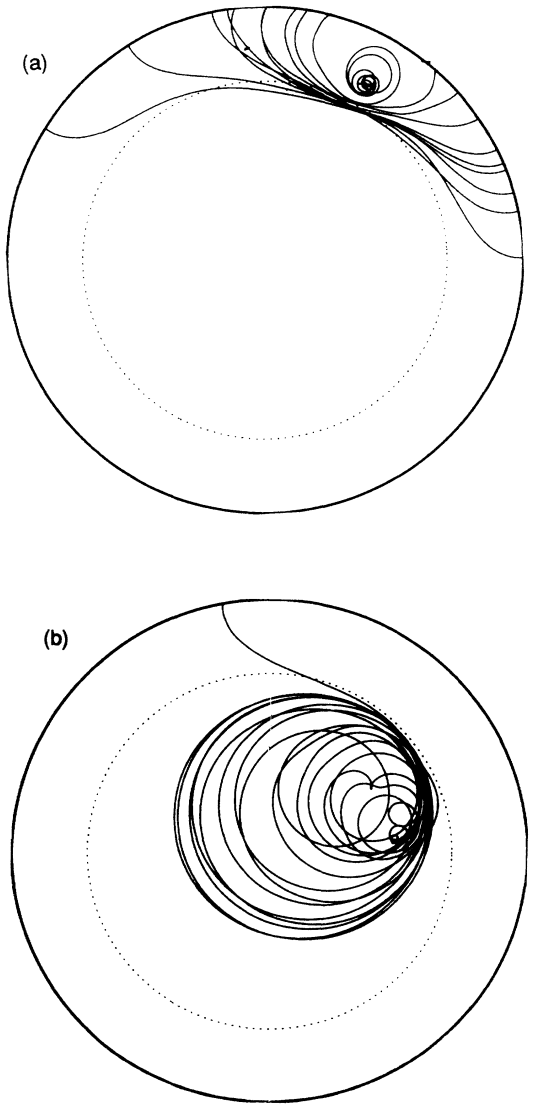

FIG. 11. (a) Spanwise view of an inflow vortex generator producing unpinned vortex generators in the outer section of the pipe ($r = 0.8\ R$). In this picture the inflow vortex generator has produced nine unpinned vortex generators. The dotted line denotes the nodal surface. All the simulation parameters are the same as in Fig. 3. (b) Spanwise view of an inflow vortex generator in the inner section of the pipe ($r = 0.5R$). No unpinned generators are produced.

ty profile. This distance is approximately[21]

$$\frac{Y}{R}\approx\frac{2\,\mathrm{Re}}{15}\ . \tag{20}$$

This equation will hold for the normal fluid. We will ignore the entry length of the normal fluid for two reasons. First, the normal-fluid density (and therefore the normal-fluid Reynolds number Re_n and the entry length Y_n) decreases rapidly with decreasing temperature. Second, the inflow vortex generator typically forms the unpinned vortex generator far downstream. Since we are only concerned in this paper with the behavior of the unpinned vortex generators, we consider the normal-fluid velocity profile to be parabolic everywhere. However, a more complete understanding of the inflow vortex generator may require that the normal-fluid entry length be taken into account.

Since the unpinned vortex generators require some time to form the arrays of vortex rings that give the superfluid a parabolic velocity profile, there is an equivalent to the classical entry length for the superfluid. To find an approximate value for this superfluid entry length, we begin with the number of vortex rings per unit length formed by the unpinned vortex generators:

$$n_{\mathrm{rings}}(t)=n_{\mathrm{UVG}}ft=n_{\mathrm{UVG}}fy/V_s\ , \tag{21}$$

where n_{UVG} is the number of unpinned vortex generators per unit length, f is the frequency of ring production per unpinned vortex generator, t is time, y is the downstream distance, and V_s is the average superfluid velocity over the position of the unpinned vortex generator. As the vortex-ring array forms and the superfluid velocity near the wall drops (Fig. 9), V_s will decrease. Though we have not measured f as the superfluid wall velocity drops, it is reasonable to expect that it also decreases, since the unpinned-vortex-generator growth is driven by the relative velocity at the wall. For this rough approximation, we will consider the ratio f/V_s to be constant through the formation of the vortex-ring array. Also, for simplicity, we will only consider the case of equal superfluid and normal-fluid average velocities $V_s=V_n\equiv V_0$.

The number density of unpinned vortex generators may be approximated by

$$n_{\mathrm{UVG}}\approx N_{\mathrm{IVG}}/\lambda\ , \tag{22}$$

where N_{IVG} is the number of inflow vortex generators in the pipe and λ is the wavelength of the growing helical wave on the inflow vortex generator. For N_{IVG} we should only count the inflow vortex generators in the outer section of the pipe cross section, between the nodal surface and the pipe wall, since these are the only inflow vortex generators which will generate unpinned vortex generators (Fig. 11). We will take λ to be the most unstable wavelength of the helical instability of a streamwise vortex filament in a flow with relative velocity V_{ns},[15,22]

$$\lambda=4\pi\beta/V_{ns}\ , \tag{23}$$

where $\beta=(\kappa/4\pi)\ln(\lambda/2\pi a_0)$. Since the logarithmic dependence is very weak, we will take β to be a constant. It should be noted that here V_{ns} is the relative velocity at the position of the inflow vortex generator. Combining Eqs. (22) and (23) with Eq. (21) gives

$$n_{\mathrm{rings}}(y)=\frac{N_{\mathrm{IVG}}fyV_{ns}}{4\pi\beta V_0}\ . \tag{24}$$

The number density of vortex rings required for the superfluid velocity profile to match the normal-fluid velocity profile is

$$n_{\mathrm{rings}}=\int_0^R\omega_n\,dr/\kappa=2V_0/\kappa\ , \tag{25}$$

where ω_n is the normal-fluid vorticity. Using Eq. (25) in Eq. (24) and solving for y gives us the superfluid entry length Y_s:

$$Y_s=\frac{8\pi\beta V_0^2}{\kappa N_{\mathrm{IVG}}fV_{ns}}\ . \tag{26}$$

In order to compare Y_s to the classical value [Eq. (20)], we rewrite it in terms of the Reynolds number [Eq. (7)],

$$\frac{Y_s}{R}=8\pi\left[\frac{\eta}{\rho\kappa}\right]\left[\frac{\tilde{V}_0}{\tilde{f}\,\tilde{V}_{ns}N_{\mathrm{IVG}}}\right]\mathrm{Re}\ , \tag{27}$$

where we have also nondimensionalized the variables using the scaling given in Eqs. (5) and (6). Assuming that the inflow vortex generators are randomly distributed across the cross section of the intake, the average V_{ns} at the inflow vortex generator is $V_0/2$. Using the ratio of the kinematic viscosity to the quantum of circulation, $\eta/\rho\kappa\approx0.1$, we can write the superfluid entry length as

$$\frac{Y_s}{R}\sim\left[\frac{5}{\tilde{f}N_{\mathrm{IVG}}}\right]\mathrm{Re}\ . \tag{28}$$

The nondimensionalized frequency $\tilde{f}$ is of order 5–10. The value of N_{IVG} is unknown, but Schwarz[15] states that in his simulations of pure superflow turbulence a minimum of three inflow vortex generators is needed in order to form a self-sustaining vortex tangle. If we compare our estimate of the superfluid entry length with the classical value [Eq. (20)], we find that an N_{IVG} on the order of 5 would make Y_s similar to the classical value. Any similarity that does exist between these values is purely coincidence due to the value of the ratio $\eta/\rho\kappa$ and should not be confused with any active process such as the motion of the vortex rings, which gives the superfluid a classical velocity profile.

VIII. CONCLUSIONS

We have shown that for helium II flows with $\mathbf{V}_n$ and $\mathbf{V}_s$ parallel, a single vortex filament attached to the boundary of a pipe with circular cross section can form a large number of superfluid vortex rings oriented with the flow. These rings are formed in an ordered manner and easily combine into large arrays of organized superfluid vortex filaments which give the superfluid velocity a parabolic profile matching the normal-fluid velocity profile at length scales larger than the filament spacing.

The operation of this vortex generator is due to the

presence of a surface in the fluid where $\mathbf{V}_n = \mathbf{V}_s$ (a nodal surface). The circular cross section of the pipe facilitates the generator operation by allowing the legs of a single vortex generator to interact and produce a vortex ring, but this special geometry is not *essential* to this behavior. As we have shown (Fig. 5), multiple generators can interact to form the vortex rings, and so the self-interaction of a single generator is not necessary. The necessary characteristic of the flow is the presence of the nodal surface which serves as a collection area for ordered superfluid vortex filaments. Analogs of the vortex generator described here for pipe flow should exist in many other flow geometries which contain such nodal surfaces. Some likely examples are channel flow, plane and cylindrical Couette flows, and the flow between the plates of a rotating Andronikashvili pendulum.

Since the function of the nodal surface is to hold and orient a superfluid vortex filament, the dimension of the surface may be as small as one dimensional. With this in mind, we propose two necessary conditions for the formation of a velocity matched flow of helium II. These conditions are the following.

(i) A region of locally matched velocity $\mathbf{V}_n = \mathbf{V}_s$ of dimension 1 or greater must initially exist in the flow.

(ii) A source of superfluid vortex filament must be present.

In the example of pipe flow treated in this paper, condition (ii) was provided for by the velocity difference $\mathbf{V}_n - \mathbf{V}_s$ at the boundary of the pipe. Solid boundaries are very convenient for this purpose for two reasons. First, even in quiescent helium, superfluid vortex filaments are likely to be found at solid boundaries in the form of remnant vortices pinned to surface roughness.[8] Second, the solid boundary forms a convenient sink for any superfluid vortex filaments with the wrong sign of circulation (opposite to the normal-fluid circulation). It is not inconceivable, however, that the superfluid vortex filament may grow in the free fluid without boundaries. If that is so, the same general process described in this paper for laminar pipe flow may also explain velocity matching in turbulent helium II flows away from boundaries.

ACKNOWLEDGMENTS

I thank Professor R. J. Donnelly and Professor W. F. Vinen for helpful comments on early versions of this paper.

[1]S. S. Courts and J. T. Tough, Phys. Rev. B **39**, 8924 (1989).
[2]P. L. Walstrom, J. G. Weisend II, J. R. Maddocks, and S. W. Van Sciver, Cryogenics **28**, 101 (1988).
[3]H. Borner and D. W. Schmidt, in *Flow of Real Fluids,* edited by G. E. A. Meier and F. Obermeier (Springer-Verlag, Berlin, 1985), p. 135.
[4]K. W. Schwarz, Phys. Rev. B **38**, 2398 (1988).
[5]J. T. Tough, in *Progress in Low Temperature Physics,* edited by D. F. Brewer (North-Holland, Amsterdam, 1982), Vol. VIII, p. 133.
[6]R. J. Donnelly and C. E. Swanson, J. Fluid Mech. **173**, 387 (1986).
[7]R. J. Donnelly, in *High Reynolds Number Flows Using Liquid and Gaseous Helium,* edited by R. J. Donnelly (Springer-Verlag, New York, 1991), p. 3.
[8]K. W. Schwarz, Phys. Rev. B **31**, 5782 (1985).
[9]R. M. Bowley, J. Phys. C **17**, 595 (1984).
[10]D. D. Awschalom and K. W. Schwarz, Phys. Rev. Lett. **52**, 49 (1984).
[11]E. L. Andronikashvili and Y. G. Mamaladze, Rev. Mod. Phys. **38**, 567 (1966).
[12]Z. Peradzynski, S. Filipkowski, and W. Fiszdon, Eur. J. Mech. B **9**, 259 (1990).
[13]S. S. Courts and J. T. Tough, Phys. Rev. B **38**, 74 (1988).
[14]W. I. Glaberson and R. J. Donnelly, Phys. Rev. **141**, 208 (1966).
[15]K. W. Schwarz, Phys. Rev. Lett. **64**, 1130 (1990).
[16]G. K. Batchelor, *An Introduction to Fluid Dynamics* (Cambridge University Press, Cambridge, England, 1967), p. 523.
[17]L. J. Campbell and R. M. Ziff, Phys. Rev. B **20**, 1886 (1979).
[18]D. Stauffer and A. L. Fetter, Phys. Rev. **168**, 156 (1968).
[19]J. A. Geurst, Phys. Lett. **71A**, 78 (1979).
[20]W. de Haas and H. van Beelen, Physica **83B**, 129 (1976).
[21]D. J. Tritton, *Physical Fluid Dynamics* (Van Nostrand Reinhold, Berkshire, 1977), p. 12.
[22]J. R. Torczynski, Phys. Rev. B **39**, 2165 (1989).